NIH Public Access
Author Manuscript
Neuron. Author manuscript; available in PMC 2010 February 12.

Published in final edited form as:
Neuron. 2009 February 12; 61(3): 412–424. doi:10.1016/j.neuron.2008.12.029.

Snapin facilitates the synchronization of synaptic vesicle fusion

Ping-Yue Pan[1,2], **Jin-Hua Tian**[1], and **Zu-Hang Sheng**[1]

1 *Synaptic Function Section, The Porter Neuroscience Research Center, National Institute of Neurological Disorders and Stroke, National Institutes of Health, Building 35, Room 3B203, 35 Convent Drive, Bethesda, Maryland 20892-3701, USA*

2 *Department of Neurobiology, School of Medicine, Shanghai Jiaotong University, Shanghai 200025, China*

Abstract

Synaptic vesicle (SV) fusion is a fine-tuned process requiring a concert of fusion machineries. Using cortical neurons from *snapin*-deficient mice, we reveal a role for Snapin in facilitating synchronous release. In addition to reduced frequency of miniature excitatory synaptic currents (mEPSCs) and smaller size of release-ready vesicle pool (RRP), *snapin* deficiency results in EPSCs with multiple peaks and increases the rise and decay times, reflecting the "desynchronized" SV fusion. These defects impair both synaptic precision and efficacy during sustained neurotransmission. Transient expression of Snapin not only rescues the slowed kinetics of EPSCs, but also further accelerates the rate found in (+/+) neurons. Furthermore, expression of Snapin-C66A, a dimerization-defective mutant with impaired interactions with SNAP-25 and Synaptotagmin, reduces the RRP size but exhibits less effect on synchronized fusion. Our studies provide mechanistic insights into a dual-role of Snapin in enhancing the efficacy of SV priming and in fine-tuning synchronous SV fusion.

Keywords

synaptotagmin; SNARE; synaptic vesicle priming; synaptic transmission; cortical neurons; exocytosis; excitatory synaptic currents; synchronization

Introduction

Information coding in the brain depends on the timing of action potentials, which is influenced by integration of unitary excitatory inputs. The size and shape of excitatory postsynaptic currents (EPSCs) are two decisive factors in tuning the temporal and spatial precision of spiking (Cathala et al., 2003; Cadetti et al., 2005) and can be modulated by presynaptic mechanisms. Ca^{2+}-triggered neurotransmitter release depends on the presence of a pool of primed release-ready synaptic vesicles (SVs) (see review by Rettig and Neher, 2002), which determines the release probability of a synapse (Zucker. 1996). The priming step corresponds to the assembly of the SNARE complex in which synaptobrevin (VAMP) interacts with SNAP-25 and syntaxin-1 to form a metastable structure before fusion (Sudhof, 2004; Wojcik and Brose, 2007). Several SNARE regulatory proteins, including Munc-18 (Hata et al., 1993), Munc 13–1 (Brose et al., 2000) and RIM1 (Betz et al., 2001; Schoch et al., 2002), Complexins (Reim et

Correspondence should be addressed to Zu-Hang Sheng at Tel: 301-435-4596; Fax: 301-480-5763; E-mail: shengz@ninds.nih.gov.

Publisher's Disclaimer: This is a PDF file of an unedited manuscript that has been accepted for publication. As a service to our customers we are providing this early version of the manuscript. The manuscript will undergo copyediting, typesetting, and review of the resulting proof before it is published in its final citable form. Please note that during the production process errors may be discovered which could affect the content, and all legal disclaimers that apply to the journal pertain.

NIH-PA Author Manuscript
NIH-PA Author Manuscript
NIH-PA Author Manuscript

NIH-PA Author Manuscript

NIH-PA Author Manuscript

NIH-PA Author Manuscript

al., 2001; Tang et al., 2006; Huntwork and Littleton) and CAPS (Jockusch et al., 2007; Liu et al., 2008), are implicated in this priming process and influence the size of EPSCs.

While much attention in the past decade has been given to the SNARE-regulatory proteins in studying SV release probability and short-term plasticity, our understanding of the molecular mechanisms that govern the tuning of EPSC shape is largely lacking. The synchronicity of vesicle fusion at the presynaptic terminal is a key determinant of the time course of AMPA receptor-mediated EPSCs (Diamond and Jahr, 1995). Therefore, identifying proteins essential for synchronous fusion provides both molecular and physiological insights into how synaptic transmission is regulated. Maturation of SVs into a release-ready state requires synaptotagmin I (Syt I), a main Ca^{2+} sensor of fast neurotransmission (see review by Chapman, 2008). The accurate assembly of Syt I-SNARE fusion machineries is critical for the precise timing of fast release within sub-milliseconds (Kesavan et al., 2007). Ca^{2+}-dependent and independent interactions between Syt I and SNAREs (Melia et al., 2002; Zhang et al., 2002; Bhalla et al., 2006) suggest that before the Ca^{2+} trigger, a loose pre-fusion Syt I-SNARE complex is assembled during the priming process. Localized Ca^{2+} influx sensitizes the Ca^{2+} sensor Syt I and induces its subsequent tight coupling to the SNARE complex (Fernandez-Chacon et al., 2001; Zhang et al., 2002; Maximov and Südhof, 2005). Mutation studies indicate that fusion pore dynamics might be changed if Syt I and SNAREs were less tightly coupled (Bai et al., 2004). Complexins have been reported to activate or clamp fusion of SVs by freezing the SNARE complex in its metastable state before Ca^{2+} influx (Tang et al., 2006; Giraudo et al., 2006; Huntwork and Littleton, 2007). In both *syt I null* neurons and neurons with elevated synaptic concentration of Complexin, the fast release was almost abolished (Maximov and Südhof, 2005; Tang et al., 2006), indicating that the proper structural coupling of Syt I with SNAREs is critical for fast SV exocytosis. These findings support a model in which Syt I synchronizes fusion at least in part by interacting with SNAREs. However, aside from the established roles of Complexins and Syt I, the regulatory mechanisms underlying synchronous SV fusion are unclear.

We initially identified Snapin as a SNAP-25-binding protein that enhances the association of Syt I with the SNAREs (Ilardi et al., 1999). Using *snapin* knockout (KO) mice, we further demonstrated that Snapin modulates fast exocytosis (exocytotic burst) of large dense-core vesicles (LDCVs) in chromaffin cells by stabilizing the structural coupling of Syt I to the SNARE complex (Tian et al., 2005). Deletion of *snapin* leads to a marked reduction in the amount of Syt I-SNARE complex in mouse brain. We now report a novel function of Snapin in synchronizing SV fusion at central synapses, where precise timing is most critical for proper synaptic function. By recoding synaptic transmission between cultured cortical neurons from *snapin*-deficient mice, we found that *snapin* mutant neurons not only have a smaller primed SV pool size, but also exhibit EPSCs with unexpected multiple peaks and fail to follow sustained firing at high frequencies. Re-introducing *snapin* into the mutant presynaptic neurons effectively accelerates the EPSC kinetics to the greater extent found in (+/+) neurons by boosting the synchronicity of SV fusion. EPSC kinetics is correlated in rank order to the relative Snapin expression level in the presynaptic neurons. Thus, our studies reveal the significance of Snapin as a unique “synchronizer” of calcium-triggered SV fusion at central nerve terminals.

Results

Snapin-deficient neurons display a reduced frequency of miniature synaptic currents and a smaller size of readily releasable pool

To define the role of Snapin in synaptic transmission at central synapses, we first compared basic synaptic properties of cultured cortical neurons from *snapin* mutant mice and their littermate controls. Whole-cell patch clamp was performed to record miniature (mini) synaptic currents in the presence of 1μM TTX at DIV10 (Figure 1A). The mean frequency of mini

NIH-PA Author Manuscript

NIH-PA Author Manuscript

NIH-PA Author Manuscript

currents decreased in a *snapin* gene dose-dependent manner (Figure 1B). Wild-type neurons had a mini frequency of 1.94 ± 0.26 Hz, whereas those in *snapin* (−/−) and (+/−) neurons were 0.45 ± 0.10 Hz and 1.06 ± 0.19 Hz, respectively. Cumulative frequency distribution of inter-event intervals revealed rightward shifts for both (−/−) and (+/−) neurons (Figure 1B, lower left), consistent with a comparable reduction in mini frequency. However, no observable difference in mini amplitude was seen (Figure 1B, right panels). Closer examination of the mini AMPA events recorded in 50 μM picrotoxin and 50 μM APV revealed no difference in average rise time (+/+, 2.84 ± 0.12 ms; −/−, 2.54 ± 0.17 ms, $p>0.05$) and decay time (+/+, 6.46 ± 0.31 ms; −/−, 5.64 ± 0.49 ms, $p>0.05$)(Figure 1C and D), suggesting that the kinetics of AMPA receptor-mediated mini-EPSC were not altered by s*napin* deletion. We further examined the release-ready vesicle pool (RRP) at the nerve terminal by applying hypertonic sucrose solution. Hypertonic responses were significantly decreased in both *snapin* (+/−) ($11.25 \pm 1.54 \times 10^4$ pA*ms, p=0.0038) and (−/−) ($12.03 \pm 2.46 \times 10^4$ pA*ms, p=0.0026) neurons compared to their wild-type controls ($19.28 \pm 2.25 \times 10^4$ pA*ms) (Figure 1E and F), suggesting smaller RRP size at the *snapin*-deficient presynaptic boutons.

Homozygous but not heterozygous deletion of *snapin* reduces presynaptic density of the cultured neurons

To examine possible changes in synapse maturation resulting from *snapin* deletion, we analyzed the densities of both total and activatable synapses. First, by co-staining neurons in culture with presynaptic marker Synapsin I and dendritic marker MAP2, we observed a modest reduction in the density of total synapses along dendrites of *snapin* (−/−) cultures (0.21 ± 0.02/μm, p=0.03) compared to (+/−) mutant (0.26 ± 0.02/μm) and (+/+) control neurons (0.27 ± 0.02/μm) from the same litter (Figure 2A and 2B). In addition, we measured active presynaptic boutons by loading the nerve terminals with FM 4–64 dye using 50 mM K^+ solution. Comparing all three genotypes of neurons revealed reduced FM 4–64 staining along axons in *snapin* (−/−) neurons (0.20 ± 0.02/μm, p=0.0009), while that in *snapin* (+/−) (0.30 ± 0.03/μm) neurons remained unchanged relative to wild type controls (0.31 ± 0.02/μm) (Figure 2C and 2D).

We next looked at the ultrastructure of the synapse from cultured neurons at the same developmental age (DIV10) when recordings were performed (Figure 2E). No changes were observed between *snapin* (+/−) (n=27) and (+/+) (n=27) neurons in the average length of active zone (AZ), the space of the synaptic cleft, vesicle diameter, number of docked vesicles per AZ length, and number of total vesicles per terminal area. However, there were fewer SVs found in (−/−) presynaptic boutons (n=7), although AZ length, space of the cleft and vesicle size remained similar to (+/+) controls (Figure 2F). Altogether, homozygous deletion of *snapin* resulted in reduced densities of total and active presynaptic boutons and reduced SVs at AZs, while in the heterozygous neurons these changes were not significant. These morphological observations suggest that, although reduced Snapin in (+/−) neurons is sufficient for synaptic maturation, its physiological expression in *snapin* (+/+) neurons might be essential to effectively regulate SV priming and fusion.

Snapin deficiency resulted in smaller size and slower kinetics of EPSCs

We next examined evoked synaptic responses by recording paired cortical neurons in *snapin* (+/+), (+/−) and (−/−) cultures (Figure 3A). Since glutamatergic synapses are the main information carriers in the cortex, here we focused our analysis on excitatory neuronal transmission. Particularly, with 2 mM Mg^{2+} in the recording bath, the EPSCs recorded under voltage clamping at −70 mV were mainly mediated by AMPA receptors. In parallel with the remarkable decrease in mini frequency, the peak amplitude of EPSCs from *snapin* (−/−) neurons showed 63.57 ± 5.75 % reduction compared to that from (+/+) neurons (Figure 3B, left). A similar reduction (51.84 ± 7.61 %) in total charge transfer was also noticed in *snapin*

NIH-PA Author Manuscript

NIH-PA Author Manuscript

NIH-PA Author Manuscript

(−/−) neurons. These results agree with the previous observation of a decreased exocytotic burst and a smaller readily releasable pool (RRP) in *snapin* (−/−) chromaffin cells (Tian et al, 2005).

Surprisingly, we also observed a profound change in the shape of EPSCs from both *snapin* (+/−) and (−/−) neurons. While a smooth and single-peaked EPSC reflecting synchronized vesicle fusion was consistently recorded from *snapin* (+/+) neurons, multi-peaked EPSCs with prolonged time course were predominantly found in both *snapin*-deficient (+/−) and (−/−) neurons (Figure 3A). The total number of peaks within a 100-ms window (analyzed by "Mini Ananlysis" software) revealed a significant increase in both *snapin* (+/−) (1.85 ± 0.15, n=16, p=0.004) and (−/−) neurons (2.01± 0.24, n=10, p=0.003) relative to that of *snapin* (+/+) control (1.20 ± 0.07, n=12) (Figure 3B, right). However, by measuring the first peak of each single trace, we found a similar rise time of the first EPSC peak between (−/−)(2.50 ± 0.37 ms) and (+/+) neurons (2.52 ± 0.41 ms, p>0.05) (Figure 3A, right). EPSC kinetics has been widely used as a sensitive metric for reflecting small changes in synaptic glutamate transients (Diamond and Jahr, 1995). We further averaged the time course of EPSCs recorded at 0.1 Hz from all genotypes of neurons (+/+, n=ε; +/−, n=13; and −/−, n=12) and scaled the peak amplitude of (+/−) and (−/−) currents to that of (+/+) EPSC (Figure 3C). Significant increases were noticed in *snapin* (−/−) neurons in EPSC half-width (+/+, 8.36 ± 0.57 ms; −/−, 11.52 ± 1.16 ms, p=0.020), 10–90% rise time (+/+, 2.87 ± 0.25 ms; −/−, 4.79 ± 0.31 ms, p<0.001), time of delay (+/+, 4.35 ± 0.33 ms; −/−, 7.65 ± 0.46 ms, p<0.001) and 10–90% decay time (+/+, 15.97 ± 1.42 ms; −/−, 25.54 ± 4.06 ms, p=0.028), representing a remarkable slow down of EPSC kinetics compared to wild-type controls (Figure 3D). The neurons with heterozygous deletion of *snapin* also exhibited relatively slowed EPSC with a significant change in decay time (21.20 ± 2.34 ms, p=0.044). Since the kinetics of AMPA mini-EPSCs remained similar between *snapin* (+/+) and (−/−) neurons (Figure 1C, D) and the rise time of the first EPSC peak recorded in (−/−) neurons was unaltered (Figure 3A, right), the observed change in averaged EPSC kinetics was unlikely due to altered AMPA receptor kinetics or delays in single vesicle fusion kinetics, but rather attributed to the failure of synchronous SV fusion.

Snapin deficiency impairs the precision and efficacy of synaptic transmission under high-frequency stimulations

To define the role of Snapin in high-frequency neuronal activity, we delivered pulse trains to the presynaptic neuron of a connected pair. EPSCs recorded from *snapin* (+/+) neurons displayed smooth depression and accurate phase-lock of the peak time to their stimuli under both 10 Hz and 50 Hz (Figure 4A and 4B). However *snapin* (+/−) and (−/−) neurons exhibited impaired responses to the high-frequency trains. Although the average rates of synaptic depression remained similar among all genotypes of neurons under 10 Hz stimulation (data not shown), the precise phase-lock was no longer observed in both *snapin* (+/−) and (−/−) neurons after the first three stimuli; additionally, the size and peak time of EPSCs became highly variable (Figure 4C). The impairment in synaptic efficacy was more evident at higher stimulation frequencies. *Snapin* (+/−) neurons displayed much faster decay in EPSC amplitudes at 50 Hz (Figure 4D) and a significant decrease in total charge transfer (+/+, n=6, 4.21 ± 1.66 × 10^4 pA*ms; +/−, n=6, 1.27 ± 0.32 × 10^4 pA*ms. p=0.02, M-W *u* test), indicating a smaller pool of release-ready SVs at the terminals although the average number of docked vesicles and gross morphology of presynaptic boutons are not significantly affected in *snapin* (+/−) neurons (Figure 2E and 2F). S*napin* null-mutation caused a more severe impairment in synaptic transmission at this stimulation rate. Due to the prolonged synaptic delay and increased EPSC rise and decay time (Figure 3C and 3D), the first EPSC was unable to return to baseline within a 20-ms interval and subsequent synaptic responses were hardly observed (Figure 4B and 4D). These results further indicate the importance of Snapin in maintaining synaptic precision and efficacy during repetitive firing.

NIH-PA Author Manuscript

NIH-PA Author Manuscript

NIH-PA Author Manuscript

Elevated external calcium partially rescues the size but not the kinetics of EPSC

Given the importance of calcium sensing during neurotransmission, we next sought to determine the distinct effect of calcium and Snapin in shaping EPSCs. Changes in Ca channel density and function could be one cause for the striking phenotypes we observed in *snapin*-deficient neurons. We recorded the calcium currents mediated by Ca channels (both N-type and P/Q type) at the soma, by giving stepwise depolarization from −40 to +60 mV. *Snapin*-deficient (+/−) neurons, in which desynchronized fusion was consistently observed, displayed similar Ca current density and activation and inactivation rates compared to wild-type neurons (Supplemental Figure 1).

To further determine the calcium sensitivity in mediating synaptic transmission, neurons from all three genotypes were first recorded at 0.1 Hz stimulations in bath solution containing 2 mM Ca^{2+}. After a period of stable recording, the same stimulation was given when neurons were perfused with 6 mM Ca^{2+} (Figure 5A). Similar folds of increase in EPSC size and charge were observed in all genotypes of neurons following the elevation of $[Ca^{2+}]_{ext}$ (Figure 5B), indicating unaltered calcium dependence for SV fusion in the lack of Snapin. A detectable effect of elevated $[Ca^{2+}]_{ext}$ was the smoothing of the EPSC shape. The number of peaks in *snapin* (+/−) and (−/−) neurons within a 100-ms window was reduced to the level of *snapin* (+/+) neurons (1.11 ± 0.07 for +/+; 1.34 ± 0.13 for +/−; and 1.20 ± 0.08 for −/−) (Figure 5C). However, more importantly, the slow EPSC kinetics from (−/−) neurons was not at all rescued by $[Ca^{2+}]_{ext}$ elevation (Figure 5D). Paired comparison showed that the changes in $[Ca^{2+}]_{ext}$ have no significant effect on the half-width, rise and decay time of EPSCs (Figure 5E), suggesting that elevated local $[Ca^{2+}]$ was insufficient to rescue the slow kinetics of EPSC or the "desynchronized" fusion in *snapin*-deficient neurons. Thus, the disappearance of additional peaks under elevated $[Ca^{2+}]_{ext}$ conditions was not due to repression of asynchronous release, but rather, to an increased signal-to-noise ratio since more SVs were sensitized for fusion.

Snapin fine-tunes EPSC kinetics in a gene-dose dependent manner

We further verified the role of Snapin in synchronous fusion at presynaptic terminals by introducing *Snapin* transgene into the cultured *snapin* (+/−) and (−/−) neurons. Recordings were obtained from the untransfected postsynaptic neuron receiving input from the pIRES-EGFP-Snapin transfected presynaptic neuron under a fluorescent microscope. A dramatic speed-up of EPSC kinetics was observed when exogenous Snapin was transiently expressed in the presynaptic neuron for 3 days, regardless of the deficiency of endogenous Snapin. Elevating Snapin expression not only rescued the slowed kinetics of EPSCs found in (+/−) and (−/−) neurons, but also further accelerated the rate found in (+/+) neurons (Figure 6A), suggesting a greater synchrony of SV fusion. Consistently, the total number of EPSC peaks resulting from a single stimulus, which was significantly increased in (+/−) neurons, decreased by 37 ± 4% (p=0.0005) after the transient expression of Snapin (Figure 6B). EPSC kinetics was sensitive to Snapin-mediated regulation in a dose-dependent manner. A correlation in the rank order of decay times and half-widths in relation to the relative expression level of Snapin in the presynaptic neurons was noted (Figure 6C), highlighting a critical role of Snapin in shaping EPSC kinetics through synchronization of SV fusion. Thus, while endogenous Snapin in (+/+) neurons is sufficient for proper SV priming and normal release probability, it is still below the saturation level for maximally synchronizing synaptic vesicle fusion. These results imply two parallel effects of Snapin in the fine regulation of SV fusion and further argue against the possibility that the desynchronized fusion is due to a developmental retardation.

Snapin dimerization significantly enhances its interaction with SNAP-25 and Syt 1

Our previous analysis of brain homogenates showed that Snapin homozygous deletion and heterozygous mutants did not affect expression of a large variety of proteins involved in synaptic vesicle exocytosis (Tian et al., 2005). To examine whether the impaired precision and

NIH-PA Author Manuscript

NIH-PA Author Manuscript

NIH-PA Author Manuscript

efficacy of synaptic transmission in *snapin*-deficient neurons could be due to altered expression of other known priming and fusion proteins, we performed immnuoblot analysis of the brain homogenates of *snapin* wild-type and deficient littermates. Our results consistently indicate that *snapin* deficiency or deletion does not result in any apparent compensatory changes in the expression of SNAREs, Complexin I/II, Munc13–1, CAPS and Syt I (Suppl. Figure 2), suggesting that the phenotypes observed in *snapin*-deficient neurons are unlikely attributed to the expression defects of the above SNARE and SNARE regulatory proteins.

To provide mechanistic insights into the roles of Snapin in SV priming and synchronized fusion, we sought to identify a Snapin dominant-negative mutant for rescue experiments. A previous report using CD spectra and multi-angle laser light scattering suggests that recombinant Snapin forms a stable dimer (Vites et al., 2004). Therefore, we asked if Snapin forms a disulfide-crosslinked homodimer. To determine this, we generated Snapin-C66A mutant by substituting a single and only cysteine residue of Snapin into alanine. Purified His-tagged Snapin wild-type (WT) and its C66A mutant were separated on SDS-PAGE under non-reduced and reduced conditions and stained with Coomassie Brilliant Blue or immunoblotted with an anti-Snapin antibody. As shown in Figure 7A, the majority of Snapin WT but not its C66A mutant migrated at the apparent molecular mass of ~40 kD under non-reduced conditions while in reduced gels, they were both exclusively detected at ~20 kD. Thus, our study further identified Snapin-C66A as a dimerization-defective mutant.

To examine whether the Snapin-C66A mutant impacts its interaction with Syt I, we incubated Snapin WT or C66A mutant with rat brain homogenates followed by immunoprecipitation. Our results demonstrated that the Snapin dimerization-defective mutant has a reduced interaction with native Syt I relative to its wild-type control (Figure 7B). In addition, we performed GST pull-down assays to determine the relative binding of Snapin WT or its C66A mutant to Syt I and SNAP-25. Snapin-C66A significantly impaired its ability to stably interact with both Syt I and SNAP-25 *in vitro* by 66% and 70%, respectively (Figure 7C-E). It is likely that the dimer structure enables Snapin to interact simultaneously with both Syt I and SNAP-25, and thus stabilizes the prefusion complex for efficient SV priming. To examine Snapin dimerization with respect to Ca^{2+} sensing, we carried out two GST pull-down assays in the presence or absence of Ca^{2+}. First, when GST-Syt I was incubated with His-Snapin or its mutant, we found that elevated Ca^{2+} can efficiently rescue the binding defect of Snapin-C66A to Syt I (Figure 7F). Second, we alternatively used GST-Snapin or GST-Snapin-C66A to pull down native Syt I from rat brain homogenates and found that Ca^{2+} enhances the interaction of Snapin-C66A to Syt I to an extent similar to the binding capability of its wild type control in the absence of Ca^{2+} (Figure 7G). In contract, GST-Snapin was unable to pull down native Complexin I/II from brain homogenates, further indicating that Snapin functions via a different interaction mode with the same set of fusion core machinery (SNAREs and Syt I) shared by other well-characterized proteins including Complexins. Together our biochemical studies suggest that Snapin-C66A could serve as a dominant negative mutant for the priming process or pre-Ca^{2+} coupling between Syt I and SNAREs.

Dual-role of Snapin in synchronizing synaptic vesicle fusion and maintaining RRP size

We next compared the rescue effects of wild-type Snapin and its C66A mutant by expressing their IRES-EGFP-tagged transgene into the *snapin*-deficient presynaptic neurons. 50-Hz trains were given and the total charge transfer, as an estimate of RRP size, was measured and compared relative to (+/+) neurons with expression of the GFP vector (1.00 ± 0.19, n=9). Consistent with the estimation by hypertonic solution application (Figure 1E and 1F), normalized total charge transfer was significantly reduced in (+/−) (0.42 ± 0.06, n=11, p=0.016) neurons expressing GFP control (Figure 8A). Although over-expressing Snapin-C66A mutant in *snapin* (+/+) neurons only mildly reduced the number of release-ready vesicles (0.59 ± 0.17,

NIH-PA Author Manuscript

NIH-PA Author Manuscript

NIH-PA Author Manuscript

n=6, p=0.10), the reduction in (+/−) neurons was remarkable (0.20 ± 0.05, n=8, p=0.017) when compared to their GFP controls. Similarly, introducing Snapin-C66A resulted in faster decay at 50 Hz stimulation in both (+/+) and (+/−) neurons (Figure 8B). However, when wild-type Snapin was expressed into *snapin* (+/−) neurons, the reduced total charge transfer (0.79 ± 0.19, n=9, p=0.037) was recovered significantly (Figure 8A) consistent with the slowed decay of EPSC size (Figure 8B), suggesting a larger pool of release-ready vesicles. Given our biochemical evidence that Snapin-C66A is a dimerization-defective mutant with reduced capacity to interact with both Syt I, it could serve as a dominant negative mutant by competitively interfering with native Snapin homodimer in neurons.

Interestingly, both Snapin wild-type and C66A mutant were similarly effective in regulating EPSC kinetics (Figure 8C). Expression of both transgenes led to dramatic decreases of EPSC half-width and decay time not only in (+/−) neurons, but also in (−/−) neurons compared to their GFP controls, respectively. The slowed rise time specifically observed in (−/−) EPSCs was accelerated by approximately 30–40% when either form of Snapin was transiently expressed in the presynaptic neuron. Thus, the observed modest retardation in synaptic development in *snapin* (−/−) neurons (Figure 2) likely does not primarily contribute to the synchronization defect in SV fusion. Considering the relatively higher amount of endogenous Snapin in (+/+) neurons compared to *snapin*-deficient neurons, the boost of fusion synchrony was only modest when introducing exogenous Snapin. These observations further suggest that Snapin plays two parallel roles in SV priming and synchronous fusion. The cysteine-66 residue, critical for Snapin dimerization, is required to stabilize primed synaptic vesicles probably via interacting with the metastable SNARE complex and Syt I before Ca^{2+} sensing. However, Snapin dimer structure is not essential for synchronized fusion. Rather, monomer Snapin is sufficient for bidirectional regulation of Ca^{2+}-triggered synchronized fusion and EPSC kinetics. These rescue experiments are consistent with our biochemical observations that Ca^{2+} can efficiently boost the interaction of Snapin-C66A with both recombinant and native Syt I *in vitro* (Figure 7F and 7G). Altogether, our findings suggest that Snapin could play a dual role in enhancing the efficacy of SV priming and in fine-tuning the precision of synchronous SV fusion.

Discussion

Using *snapin*-deficient cortical neurons in combination with gene rescue experiments, we revealed a marked role of Snapin in synchronizing fast neurotransmitter release. First, deletion of *snapin* not only reduced EPSC size, but more significantly slowed EPSC kinetics. Multi-peaked EPSCs were predominantly observed in *snapin*-deficient neurons, reflecting the “desynchronized” SV fusion. Second, increased $[Ca^{2+}]_{ext}$ rescued the deficit in synaptic efficacy, while leaving defective synaptic precision unaltered. Third, elevated expression of Snapin in *snapin*-deficient presynaptic neurons efficiently restored the synchronicity of vesicle fusion and enhanced EPSC kinetics to a greater extent than that found in wild-type synapses, suggesting a non-saturated capability of Snapin-dependent regulation in normal conditions. Furthermore, Snapin dimerization via its cysteine-66 residue significantly enhanced its interaction with SNAP-25 and Syt I. In addition, Snapin WT, but not its dimerization-defective mutant C66A, rescued the reduced size of RRP. However, Snapin-C66A was sufficient for accelerating Ca^{2+}-triggered synchronized fusion in *snapin*-deficient neurons. Thus, our studies provide new mechanistic insights into a crucial dual-role of Snapin in enhancing the efficacy of SV priming and in fine-tuning the precision of synchronous SV fusion.

NIH-PA Author Manuscript

NIH-PA Author Manuscript

NIH-PA Author Manuscript

Snapin dimerization may play an essential role in stabilizing the RRP by tightly grasping SNAREs with Syt I

In addition to the core fusion proteins SNAREs and Munc18, a number of regulatory proteins have been well characterized for their roles in modulating the priming process or mediating transmitter release (see review by Rizo and Rosenmund, 2008). Deletion of Munc13-1 and -2 in mice resulted in elimination of spontaneous and evoked release (Varoqueaux et al., 2002). RIM1αknockout mice also exhibit impaired vesicle priming caused by the interruption of its binding to Munc13s (Betz et al., 2001). CAPS-1 and -2, which share homologous sequence with Munc13s, have been reported as important priming proteins for both LDCVs (Walent et al., 1992; Liu et al., 2008) and SVs (Jockusch et al., 2007). Double deletion of *caps* genes significantly decreased the RRP size and impaired fast phasic glutamate release in cultured hippocampal neurons, a defect that can be reversed by elevating intracellular Ca^{2+} levels. Studies on Complexins I/II suggested a dual-role model during the late step of transmitter release. Analysis of *Drosophila complexin* null mutants suggests that Complexin functions as the fusion clamp (Huntwork and Littleton, 2007), probably by tightly binding to SNAREs through an α-helix interaction (Reim et al., 2001; Chen et al., 2002;). However, the phenotypes observed from mammalian neurons display different features. Increasing local concentration of Complexin I impaired fast phasic transmission (Tang et al., 2006), while *complexin I and II* double knockout neurons showed reduced transmitter release with decreased Ca^{2+} sensitivity (Reim et al., 2001), leading to the hypothesis that Complexins binding to the SNARE complex generate a metastable state for Ca^{2+}-Syt I for fast release. Despite these well-established studies, protein machineries and regulators for SV synchronized fusion are yet to be fully identified.

We report here that Snapin serves as a priming protein as well. The reduced glutamate transmission and the smaller RRP size observed in *snapin*-deficient neurons are reminiscent of a priming-defective model. In s*napin* (+/−) neurons, where morphological evidence for retardation of synaptic development was not observed, decreased RRP size is likely from the defective structural or functional coupling of Syt I with SNAREs. Reintroducing wild-type Snapin into the presynaptic neurons reversed the impairment and led to larger RRP size, while expression of the dimerization-defective Snapin-C66A mutant further reduced RRP size in *snapin*-deficient neurons and resulted in faster decay at 50-Hz stimulation. These experiments support our biochemical observations that Snapin wild-type, but not its C66A mutant, bound to Syt I in the absence of Ca^{2+}, although the binding affinity with Snapin C66A was effectively boosted by Ca^{2+}. The phenotypes observed from the *snapin*-deficient neurons are also consistent with the newly emerging view regarding an alternative function of Syt I, which facilitates formation of a synaptic vesicle pool more capable of synchronous release (Voets et al., 2001; Yoshihara and Littleton, 2002; Nishiki and Augustine, 2004). Previous studies showed that Syt I was able to associate with the SNARE complex independent of Ca^{2+} in brain homogenates and such an association could be further enhanced by Ca^{2+} (Melia et al., 2002; Zhang et al., 2002; Bhalla et al., 2006; Tian et al., 2005), although it is unclear whether the Ca^{2+}-independent Syt I-SNARE complex is physiologically stable at synapses. Our biochemical observations that Snapin-C66A is functionally defective in binding to the Syt-1-SNARE complex in the absence of Ca^{2+} is consistent with the dominant negative effect by over-expressing Snapin-C66A in the *snapin* (+/−) neurons. Our study supports the notion that during the early steps of SV priming, structural coupling between Syt I and SNAREs is independent of Ca^{2+} but stabilized by Snapin dimer. Thus, Snapin dimerization may play an essential role in stabilizing the RRP by tightly grasping SNARE or t-SNARE proteins with Syt I around the fusion site prior to Ca^{2+} sensing. Upon Ca^{2+} entering the terminal during an action potential, Ca^{2+}-Syt I switches the priming mode to an accelerated fusion via changing Syt I interactions with its effector phospholipids and the SNARE complex and opening the fusion pore (Martens et al., 2007).

NIH-PA Author Manuscript

NIH-PA Author Manuscript

NIH-PA Author Manuscript

Snapin is essential for fine-tuning the precision of synchronous SV fusion

Close alignment of Syt I and SNAREs is necessary to hold the primed SVs in a hemifused state before the Ca^{2+} trigger (Martens et al., 2007; Zhang et al., 2002; Soerensen et al., 2006; Bai et al., 2004). Synchronous release might demand more energy from the SNARE machinery than asynchronous release (Kesavan et al., 2007), probably due to Complexin-mediated arrest of SV fusion in a hemifused state (Tang et al., 2006; Giraudo et al., 2006). We now provide genetic and physiological evidence that Snapin may serve as a positive regulator in facilitating the formation of a synaptic vesicle pool more capable of synchronous release. We propose that Snapin is required to stabilize "the pre-Ca^{2+} Syt I-SNARE complex" or "the clamped intermediate", which may be essential to convert the asynchronous events into rapidly synchronous release in response to the Ca^{2+} trigger. This assumption is supported by our observations that the deletion of *snapin* leads to marked reduction in the amount of Syt I-SNARE complex *in vivo* (Tian et al., 2005) and delayed EPSC kinetics, and that recombinant Snapin enhances the interaction of Syt I and SNAP-25 *in vitro (*Ilardi et al., 1999; Chheda et al., 2001) and efficiently rescues the slowed EPSC kinetics in *snapin*-deficient neurons. Thus, at *snapin*-deficient nerve terminals, SVs are likely heterogeneously primed due to the un-favorable or un-stable association of Syt I with the metastable SNARE complex before the Ca^{2+} sensing. It leads to two defects: (1) fewer fusion competent vesicles, and hence decreased size of EPSCs; and (2) fewer vesicles undergoing synchronized fusion within a narrow time window during excitation-secretion coupling. A higher [Ca^{2+}] might sensitize more SVs for fusion, but fails to bypass the defects in the pre-fusion structural coupling between Syt I and SNAREs. Thus, it is likely that different priming proteins may play distinct roles in regulating fast neurotransmitter release. While CAPS proteins are essential components of the SV priming machinery (Jockusch et al., 2007), and Complexins activate or clamp a metastable SNARE complex at a point before Ca^{2+} triggering (Tang et al., 2006; Giraudo et al., 2006; Huntwork and Littleton, 2007), Snapin serves as a critical "stabilizer" of the pre-Ca^{2+} Syt I-SNARE complex not only for maintaining the RRP size, but also for forming Snapin-dependent RRP more capable of synchronous release. These proteins may act in parallel by fine-tuning the efficacy and precision of fast and synchronous SV fusion.

Snapin may serve as a molecular target for modifications of cortical networks and the cognitive impairments prominent in schizophrenia

Any change in EPSC kinetics could have profound influences on brain function, especially by changing spike-timing dependent plasticity. The shape of EPSCs influences synaptic integration by affecting both temporal and spatial summation at dendrites, thereby tuning neuronal firing. The marked increase in rise/decay time and synaptic latency (delay time) observed in *snapin*-deficient neurons changes the shape of the EPSC. These defects lead to an overall impairment in both synaptic efficacy and precision, especially under high-frequency stimulations, in turn altering the integration code at postsynaptic neurons. Given its non-saturated capacity in neurons, Snapin may serve as a molecular target for modifications of EPSC kinetics. This mechanism may be modulated by changing the affinity of Snapin for the Syt I-SNARE complex through PKA-dependent Snapin phosphorylation (Chheda et al., 2001; Thakur et al., 2004) or via potential oxidative stress in reducing Snapin dimerization.

Several groups discovered a direct interaction between Snapin and dysbindin (BTNBP1), the product of a susceptibility gene found among the most common genetic variations associated with schizophrenia (Starcevic and Dell'Angelica, 2004; Numakawa et al., 2004; Nazarian et al., 2006; Talbot et al., 2006; Newell-Litwa et al., 2007; Morris et al., 2008; Feng et al., 2008). Both dysbindin and Snapin associate with SVs (Talbot et al., 2006, Tian et al., 2005) and directly interact via a 30-residue sequence at dysbindin N-terminus (Feng et al., 2008). Similar to the phenotype of *sandy* mice which harbor genetic deletion of *BTNBP1* and demonstrate reduced release probability, smaller RRP size and slower kinetics of glutamate

NIH-PA Author Manuscript

NIH-PA Author Manuscript

NIH-PA Author Manuscript

release in hippocampal synapses (Chen et al., 2008), the *snapin*-deficient cortical neurons also displayed reduced RRP size and impaired synchronous neurotransmitter release. In addition, deletion of *snapin* changed EPSC shape and resulted in an inability to sustain high-frequency neuronal firing. The *sandy* mouse manifested schizophrenia-like behaviors such as social withdrawal and cognitive deficits, and in *sandy* mouse hippocampus, the steady-state level of Snapin was significantly reduced (Feng et al., 2008). In contrast, the expression of neuronal SNAREs and Syt I and other regulatory components including Munc18-1 and Complexins, or the assembly of the SNARE complex are not changed in *sandy* mouse. These findings highlight the possibility that the destabilization of Snapin in the *sandy* mouse might contribute to impaired kinetics of neurotransmission and schizophrenia-like behaviors. Since the hypofunction of glutamatergic transmission and impaired rhythmic activity within the cortical circuits have been shown to underlie some aspects of the neuropathology of schizophrenia (Tsai and Coyle, 2002; Behrendt, 2006), future study of *snapin* mutant phenotypes will provide an intriguing cellular mechanism for the cognitive impairments prominent in schizophrenia.

Methods

Culture and transfection

Cortices were dissected from E18–19 *snapin* (+/+), (+/−) and (−/−) littermates from (+/−) breeders. *Snapin* (+/−) breeders were back-crossed with C57/BL6 wild-type mice every 3–4 months to maintain well-defined genetic background while minimizing genetic drifts. Cortical neurons were dissociated by papain (Worthington) and plated on wild-type glial bed. Neurons were grown *in vitro* for at least 10–12 days (DIV 10–12) before recording, while supplemented with B27, fetal bovine serum, G-5, GlutaMAX (Invitrogen). Full-length *snapin* gene and mutant *snapin-C66A* were cloned into pIRES2-EGFP vector, and transfection was carried out at DIV 7–8 using Lipofectamine 2000 (Invitrogen). Recordings were performed 3 days after transfection.

Electrophysiology and data analysis

Dual patch-clamp recordings were made with a whole-cell configuration at room temperature to obtain EPSCs. Both neurons were voltage-clamped at −70 mV. Membrane currents were acquired using a MultiClamp 700B amplifier and digitized by Digidata 1322A with pCLAMP 9.2 software (Axon Instruments/Molecular Devices). Signals were filtered at 2 KHz. During low-frequency stimulation, a hyperpolarization step (−5 mV, 40 ms) was given at the end of the trial to monitor the steady state of input resistance. Master 8 (A.M.P.I.) was used to generate trains of high-frequency stimulations. The extracellular recording bath containing (in mM): 145 NaCl, 3 KCl, 10 HEPES, 2 $CaCl_2$, 8 Glucose, 2 $MgCl_2$ and 0.05 picrotoxin (pH 7.2, 300mOsm). Patch pipettes (Sutter Instrument) with resistance of 4–6 MΩ were tip-filled and then back-filled with pipette solution containing (in mM) 146.5 K-gluconate, 7.5 KCl, 9 NaCl, 1 $MgCl_2$, 10 HEPES, 0.2 EGTA and 2 ATP-Na_2 (pH 7.2, 300mOsm). 6 mM [Ca^{2+}] perfusion was achieved by using a circulating pump. EPSCs were recorded at least 8 min later, when they appeared steadily larger in size. For miniature current recording, 1 μM TTX was added to the recording bath. Events and number of peaks were detected and analyzed by MiniAnalysis (Synaptosoft) with uniform settings for all recordings. To evoke hypertonic responses, 700 mM sucrose in normal saline was applied by gravity flow for 5 sec, and then washed out by a circulating pump for at least 5 min. For calcium current recording, the bath solution contained (in mM) 145 NaCl, 10 HEPES, 10 $CaCl_2$, 8 Glucose, 1 $MgCl_2$, 0.001 TTX and 0.01 Nimodipine (Sigma). The pipette solution contained (in mM): 115 $CsMeSO_3$, 20 CsCl, 10 HEPES, 2.5 $MgCl_2$, 4 ATP-Na_2, 6 EGTA. Series resistance was auto-compensated; whole-cell current was acquired by pCLAMP 9.2 and filtered at 1 KHz. For significance evaluation, data sets with normal distribution were analyzed by Student *t* test. Mann-Whitney *u* test/Wilcoxon rank sum test was used otherwise.

NIH-PA Author Manuscript

NIH-PA Author Manuscript

NIH-PA Author Manuscript

Immunocytochemistry

Neurons were fixed at DIV 10–12 with a solution containing 4% formaldehyde (Polyscience Inc.), 4% sucrose (Sigma) in 1X PBS for 30 min at RT. Cell were washed 3X with 1X PBS, blocked 1 hr with 0.5% Triton X-100, 5% goat serum in 1X PBS, incubated with primary antibodies over night at 4 °C, followed by secondary antibody application (Alexa 488- or 546-conjugated) for 30 min. Antibodies used in the study include: monoclonal against SynapsinI (Synaptic System, 1:200), Synaptophysin (CHEMICON, 1:1000) and CAPS (BD Transduction Laboratory, 1:50); polyclonal against MAP2 (Santa Cruz, 1:1000); Synaptophysin (Santa Cruz, 1:800); ComplexinI/II (Synaptic System, 1:1000); and Secondary antibodies (Molecular Probes, 1:400).

Supplementary Material

Refer to Web version on PubMed Central for supplementary material.

Acknowledgements

We thank the following people for their help: J Rettig and G Chen for many insightful suggestions and comments throughout the study; D. Schoenberg, C Gerwin and C Zyskind for critical reading of the manuscript; B Lu, J Diamond, J Kang for helpful discussions; C Gerwin for mouse maintenance and genotyping. P-Y Pan is a doctoral student in the Joint Graduate Partnership Program in Neuroscience between NIH and Shanghai Jiao-Tong University, China. The work was supported by the Intramural Research Program of NINDS, NIH (Z-H. S).

References

Bai J, Wang C, Richards DA, Jackson MB, Chapman ER. Fusion pore dynamics are regulated by synaptotagmin*t-SNARE interactions. Neuron 2004;41:929–942. [PubMed: 15046725]

Behrendt R. Dysregulation of thalamic sensory “transmission” in schizophrenia: neurochemical vulnerability to hallucinations. J Psychopharmacol 2006;20:356–372. [PubMed: 16174672]

Betz A, Thakur P, Junge HJ, Ashery U, Rhee JS, Scheuss V, Rosenmund C, Rettig J, Brose N. Functional interaction of the active zone proteins Munc13-1 and RIM1 in synaptic vesicle priming. Neuron 2001;30:183–196. [PubMed: 11343654]

Bhalla A, Chicka MC, Tucker WC, Chapman ER. Ca^{2+}-synaptotagmin directly regulates t-SNARE function during reconstituted membrane fusion. Nat Struct Mol Biol 2006;13:323–30. [PubMed: 16565726]

Boudkkazi S, Carlier E, Ankri N, Caillard O, Giraud P, Fronzaroli-Molinieres L, Debanne D. Release-dependent variations in synaptic latency: a putative code for short- and long-term synaptic dynamics. Neuron 2007;56:1048–1060. [PubMed: 18093526]

Brose N, Rosenmund C, Rettig J. Regulation of transmitter release by Unc-13 and its homologues. Curr Opin Neurobiol 2000;10:303–311. [PubMed: 10851170]

Cadetti L, Tranchina D, Thoreson WB. A comparison of release kinetics and glutamate receptor properties in shaping rod-cone differences in EPSC kinetics in the salamander retina. J Physiol 2005;569:773–788. [PubMed: 16223761]

Cathala L, Brickley S, Cull-Candy S, Farrant M. Maturation of EPSCs and intrinsic membrane properties enhances precision at a cerebellar synapse. J Neurosci 2003;23:6074–6085. [PubMed: 12853426]

Chapman ER. How Does Synaptotagmin Trigger Neurotransmitter Release? Annu Rev Biochem. 2008in press

Chen X, Tomchick DR, Kovrigin E, Araç D, Machius M, Südhof TC, Rizo J. Three-dimensional structure of the complexin/SNARE complex. Neuron 2002;33:397–409. [PubMed: 11832227]

Chen XW, Feng YQ, Hao CJ, Guo XL, He X, Zhou ZY, Guo N, Huang HP, Xiong W, Zheng H, Zuo PL, Zhang CX, Li W, Zhou Z. DTNBP1, a schizophrenia-susceptibility gene, affects kinetics of transmitter release. J Cell Biol 2008;181:791–801. [PubMed: 18504299]

Chheda MG, Ashery U, Thakur P, Rettig J, Sheng ZH. Phosphorylation of Snapin by PKA modulates its interaction with the SNARE complex. Nat Cell Biol 2001;3:331–338. [PubMed: 11283605]

NIH-PA Author Manuscript NIH-PA Author Manuscript NIH-PA Author Manuscript

Diamond JS, Jahr CE. Asynchronous release of synaptic vesicles determines the time course of the AMPA receptor-mediated EPSC. Neuron 1995;15:1097–1107. [PubMed: 7576653]

Feng YQ, Zhou ZY, He X, Wang H, Guo XL, Hao CJ, Guo Y, Zhen XC, Li W. Dysbindin deficiency in sandy mice causes reduction of snapin and displays behaviors related to schizophrenia. Schizophr Res. 2008 Sep 4;[Epub ahead of print]

Fernández-Chacón R, Königstorfer A, Gerber SH, García J, Matos MF, Stevens CF, Brose N, Rizo J, Rosenmund C, Südhof TC. Synaptotagmin I functions as a calcium regulator of release probability. Nature 2001;410:41–49. [PubMed: 11242035]

Giraudo CG, Eng WS, Melia TJ, Rothman JE. A clamping mechanism involved in SNARE-dependent exocytosis. Science 2006;313:676–680. [PubMed: 16794037]

Hata Y, Slaughter CA, Südhof TC. Synaptic vesicle fusion complex contains unc-18 homologue bound to syntaxin. Nature 1993;366:347–351. [PubMed: 8247129]

Huntwork S, Littleton JT. A complexin fusion clamp regulates spontaneous neurotransmitter release and synaptic growth. Nat Neurosci 2007;10:1235–1237. [PubMed: 17873870]

Ilardi JM, Mochida S, Sheng ZH. Snapin: a SNARE-associated protein implicated in synaptic transmission. Nat Neurosci 1999;2:119–124. [PubMed: 10195194]

Jack JJ, Redman SJ. The propagation of transient potentials in some linear cable structures. J Physiol 1971;215:283–320. [PubMed: 5145721]

Jockusch WJ, Speidel D, Sigler A, Sørensen JB, Varoqueaux F, Rhee JS, Brose N. CAPS-1 and CAPS-2 are essential synaptic vesicle priming proteins. Cell 2007;131:796–808. [PubMed: 18022372]

Kesavan J, Borisovska M, Bruns D. v-SNARE actions during Ca(2+)-triggered exocytosis. Cell 2007;131:351–363. [PubMed: 17956735]

Liu Y, Schirra C, Stevens DR, Matti U, Speidel D, Hof D, Bruns D, Brose N, Rettig J. CAPS facilitates filling of the rapidly releasable pool of large dense-core vesicles. J Neurosci 2008;28:5594–5601. [PubMed: 18495893]

Martens S, Kozlov MM, McMahon HT. How synaptotagmin promotes membrane fusion. Science 2007;316:1205–1208. [PubMed: 17478680]

Maximov A, Südhof TC. Autonomous function of synaptotagmin 1 in triggering synchronous release independent of asynchronous release. Neuron 2005;48:547–554. [PubMed: 16301172]

Melia TJ, Weber T, McNew JA, Fisher LE, Johnston RJ, Parlati F, Mahal LK, Sollner TH, Rothman JE. Regulation of membrane fusion by the membrane-proximal coil of the t-SNARE during zippering of SNAREpins. J Cell Biol 2002;158:929–40. [PubMed: 12213837]

Morris DW, et al. Dysbindin (DTNBP1) and the biogenesis of lysosome-related organelles complex 1 (BLOC-1): main and epistatic gene effects are potential contributors to schizophrenia susceptibility. Biol Psychiatry 2008;63:24–31. [PubMed: 17618940]

Nazarian R, Starcevic M, Spencer MJ, DellÁngelica EC. Reinvestigation of the dysbindin subunit of BLOC-1 (biogenesis of lysosome-related organelles complex-1) as a dystrobrevin binding protein, Biochem. J 2006;395:587–598.

Newell-Litwa K, Seong E, Burmeister M, Faundez V. Neuronal and non-neuronal functions of the AP-3 sorting machinery. J Cell Sci 2007;120:531–541. [PubMed: 17287392]

Nishiki T, Augustine GJ. Synaptotagmin I synchronizes transmitter release in mouse hippocampal neurons. J Neurosci 2004;24:6127–6132. [PubMed: 15240804]

Numakawa T, et al. Evidence of novel neuronal functions of dysbindin, a susceptibility gene for schizophrenia. Hum Mol Genet 2004;13:2699–2708. [PubMed: 15345706]

Reim K, Mansour M, Varoqueaux F, McMahon HT, Südhof TC, Brose N, Rosenmund C. Complexins regulate a late step in Ca^{2+}-dependent neurotransmitter release. Cell 2001;104:71–81. [PubMed: 11163241]

Rettig J, Neher E. Emerging roles of presynaptic proteins in Ca^{++}-triggered exocytosis. Science 2002;298:781–785. [PubMed: 12399579]

Rizo J, Rosenmund C. Synaptic vesicle fusion. Nat Struct Mol Biol 2008;15:665–674.

Sabatini BL, Regehr WG. Timing of synaptic transmission. Annu Rev Physiol 1999;61:521–542. [PubMed: 10099700]

NIH-PA Author Manuscript

NIH-PA Author Manuscript

NIH-PA Author Manuscript

Schoch S, Castillo PE, Jo T, Mukherjee K, Geppert M, Wang Y, Schmitz F, Malenka RC, Südhof TC. RIM1alpha forms a protein scaffold for regulating neurotransmitter release at the active zone. Nature 2002;415:321–326. [PubMed: 11797009]

Sørensen JB, Wiederhold K, Müller EM, Milosevic I, Nagy G, de Groot BL, Grubmüller H, Fasshauer D. Sequential N- to C-terminal SNARE complex assembly drives priming and fusion of secretory vesicles. EMBO J 2006;25:955–966. [PubMed: 16498411]

Starcevic M, Dell'Angelica EC. Identification of snapin and three novel proteins (BLOS1, BLOS2, and BLOS3/reduced pigmentation) as subunits of biogenesis of lysosome-related organelles complex-1 (BLOC-1). J Biol Chem 2004;279:28393–28401. [PubMed: 15102850]

Sudhof TC. The synaptic vesicle cycle. Annu Rev Neurosci 2004;27:509–547. [PubMed: 15217342]

Talbot K, Cho D, Ong W, Benson MA, Han L, Kazi HA, Kamins J, Hahn C, Blake DJ, Arnold SE. Dysbindin-1 is a synaptic and microtubular protein that binds brain snapin. Hum Mol Genet 2006;15:3041–3054. [PubMed: 16980328]

Tang J, Maximov A, Shin O, Dai H, Rizo J, Südhof TC. A complexin/synaptotagmin 1 switch controls fast synaptic vesicle exocytosis. Cell 2006;126:1175–1187. [PubMed: 16990140]

Thakur P, Stevens DR, Sheng ZH, Rettig J. Effects of PKA-mediated phosphorylation of Snapin on synaptic transmission in cultured hippocampal neurons. J Neurosci 2004;24:6476–6481. [PubMed: 15269257]

Tian J, Wu Z, Unzicker M, Lu L, Cai Q, Li C, Schirra C, Matti U, Stevens D, Deng C, Rettig J, Sheng ZH. The role of Snapin in neurosecretion: snapin knock-out mice exhibit impaired calcium-dependent exocytosis of large dense-core vesicles in chromaffin cells. J Neurosci 2005;25:10546–10555. [PubMed: 16280592]

Tong G, Jahr CE. Multivesicular release from excitatory synapses of cultured hippocampal neurons. Neuron 1994;12:51–59. [PubMed: 7507341]

Tsai G, Coyle JT. Glutamatergic mechanisms in schizophrenia. Annu Rev Pharmacol Toxicol 2002;42:165–179. [PubMed: 11807169]

Varoqueaux F, Sigler A, Rhee JS, Brose N, Enk C, Reim K, Rosenmund C. Total arrest of spontaneous and evoked synaptic transmission but normal synaptogenesis in the absence of Munc13-mediated vesicle priming. Proc Natl Acad Sci U S A 2002;99:9037–9042. [PubMed: 12070347]

Vites O, Rhee JS, Schwarz M, Rosenmund C, Jahn R. Reinvestigation of the role of snapin in neurotransmitter release. J Biol Chem 2004;279:26251–26256. [PubMed: 15084593]

Voets T, Moser T, Lund PE, Chow RH, Geppert M, Südhof TC, Neher E. Intracellular calcium dependence of large dense-core vesicle exocytosis in the absence of synaptotagmin I. Proc Natl Acad Sci U S A 2001;98:11680–11685. [PubMed: 11562488]

Walent JH, Porter BW, Martin TF. A novel 145 kd brain cytosolic protein reconstitutes Ca(2+)-regulated secretion in permeable neuroendocrine cells. Cell 1992;70:65–75.

Wojcik SM, Brose N. Regulation of membrane fusion in synaptic excitation-secretion coupling: speed and accuracy matter. Neuron 2007;55:11–24. [PubMed: 17610814]

Yoshihara M, Littleton JT. Synaptotagmin I functions as a calcium sensor to synchronize neurotransmitter release. Neuron 2002;36:897–908. [PubMed: 12467593]

Zhang X, Kim-Miller MJ, Fukuda M, Kowalchyk JA, Martin TFJ. Ca2+-dependent synaptotagmin binding to SNAP-25 is essential for Ca2+-triggered exocytosis. Neuron 2002;34:599–611. [PubMed: 12062043]

Zucker RS. Exocytosis: a molecular and physiological perspective. Neuron 1996;17:1049–1055. [PubMed: 8982154]

NIH-PA Author Manuscript

NIH-PA Author Manuscript

NIH-PA Author Manuscript

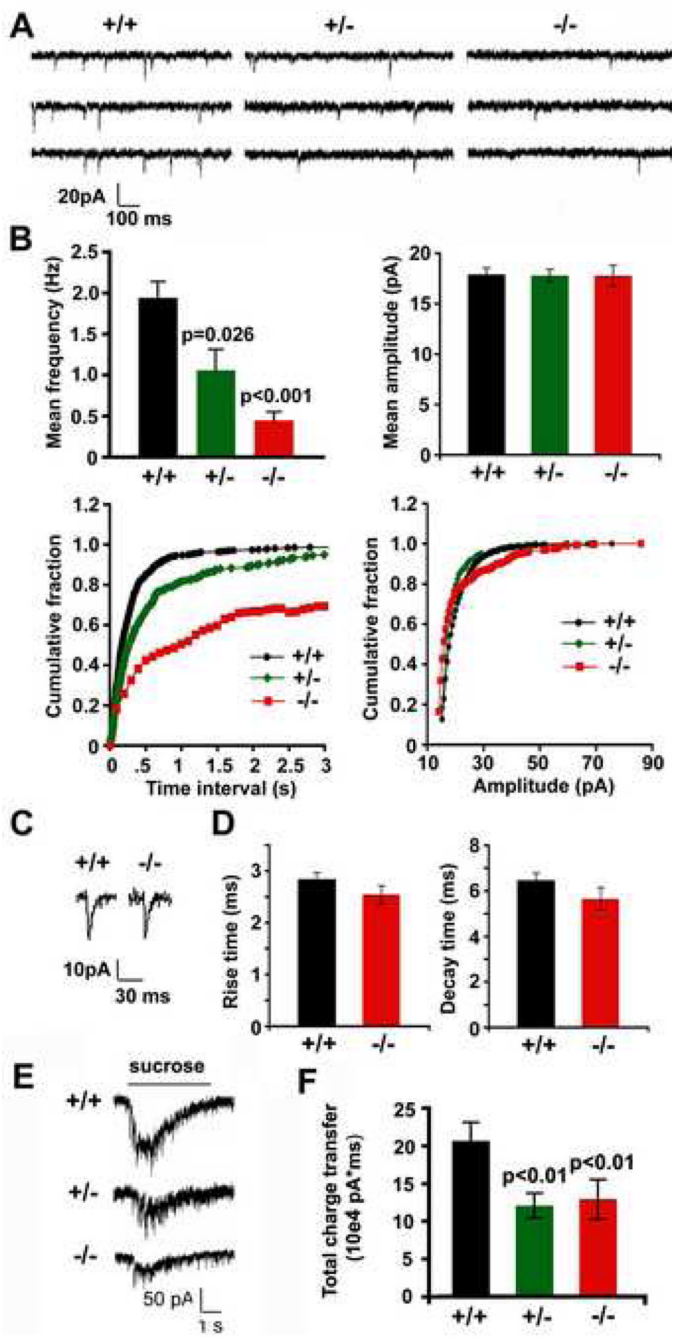

Figure 1. Snapin-deficient neurons display a reduced frequency of miniature synaptic currents and a smaller size of readily releasable pool

(A) Representative miniature currents recorded from cultured *snapin* (+/+), (+/−) and (−/−) cortical neurons at DIV10 in the presence of 1 μM TTX.

(B) Bar graphs of mean frequencies (upper left) and mean amplitudes (upper right) and cumulative distribution plots of inter-event interval (lower left) and miniature amplitude (lower right) recorded from *snapin* (+/+) (n=20), (+/−) (n=35), and (−/−) (n=20) cortical neurons, respectively. Significant differences were observed in mini frequency between (−/−) and (+/+) neurons ($p<0.001$), as well as between (+/−) and (+/+) neurons ($p=0.026$).

NIH-PA Author Manuscript

NIH-PA Author Manuscript

NIH-PA Author Manuscript

(C) Representative miniature AMPA currents isolated by 50 μM picrotoxin and 50 μM APV were recorded from *snapin* (+/+) and (−/−) cortical neurons.
(D) Bar graphs of mean rise time and decay time of mini AMPA currents recorded from *snapin* (+/+) (n=10) and (−/−) (n=9) neurons. Differences between the groups were not significant ($p>0.05$).
(E) Representative hypertonic responses from *snapin* (+/+), (+/−) and (−/−) neurons, respectively.
(F) Averaged total charge of sucrose-induced responses from (+/+) (n=18), (+/−) (n=22), and (−/−) neurons (n=15). Significant decreases were found for both (+/−) ($p=0.0038$) and (−/−) ($p=0.0026$) responses relative to (+/+) control. Error bars: s.e.m.

NIH-PA Author Manuscript
NIH-PA Author Manuscript
NIH-PA Author Manuscript

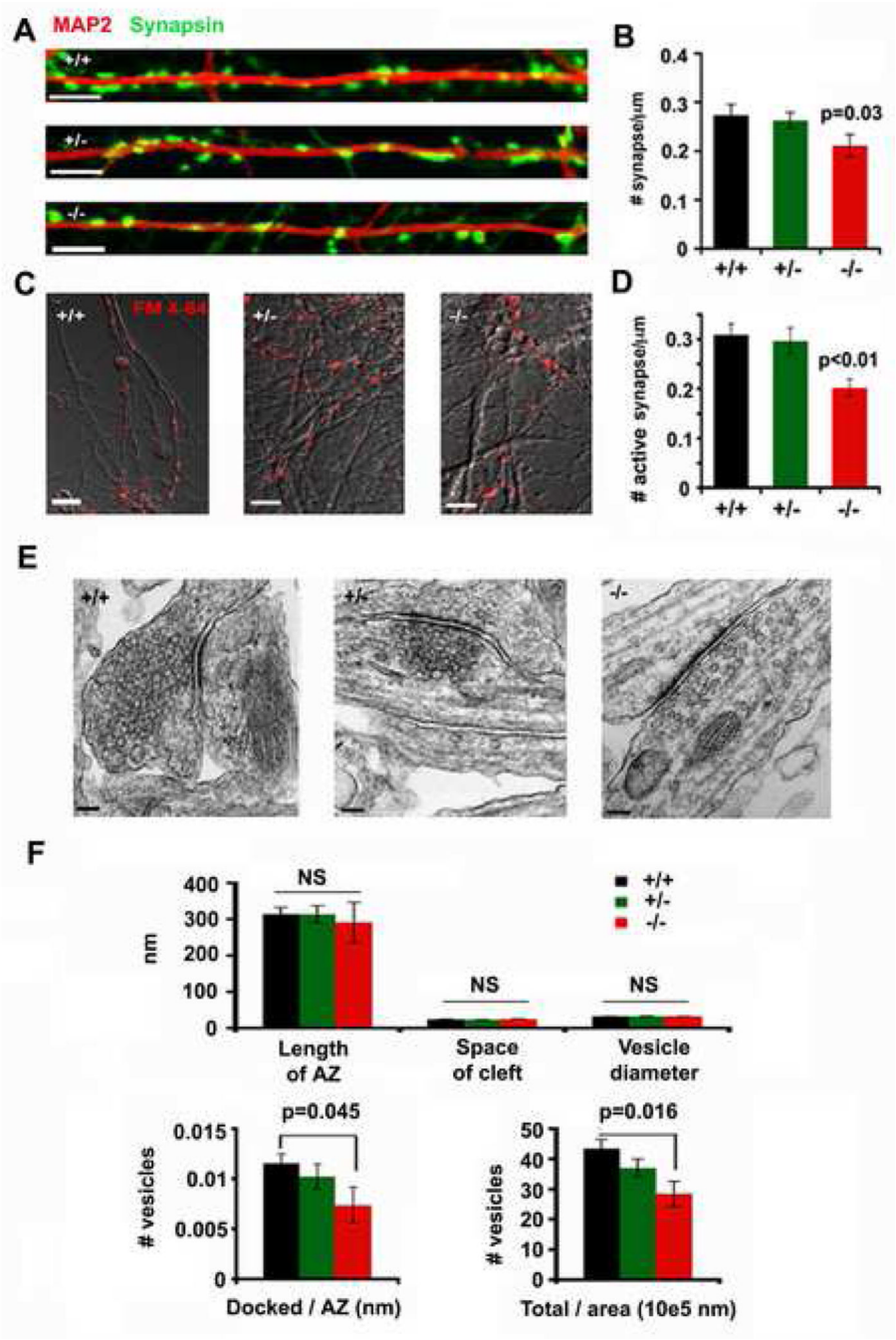

Figure 2. Homozygous but not heterozygous deletion of *snapin* reduces presynaptic density

(A) Representative images of presynaptic terminals labeled with anti-Synapsin antibody along a dendritic process marked by MAP2 from *snapin* (+/+), (+/−) and (−/−) neurons as indicated.

(B) Bar graph of averaged number of Synapsin punta per µm dendritic length for *snapin* (+/+), (+/−), and (−/−) neurons. Significant decrease (p=0.03, *t* test) was only observed in (−/−) neurons relative to (+/+) control.

(C) Representative images of active presynaptic boutons loaded with FM 4–64 from *snapin* (+/+), (+/−) and (−/−) neurons as indicated. Scale bars for A and C: 5 µm.

NIH-PA Author Manuscript

NIH-PA Author Manuscript

NIH-PA Author Manuscript

(D) Bar graph of averaged number of FM puncta (active synapse) per μm axon length for *snapin* (+/+), (+/−) and (−/−) neurons. Significant decrease (p=0.0009, *t* test) was only observed in (−/−) neurons relative to (+/+) control.
(E) Representative ultrastructural images of a synapse from cultured *snapin* (+/+), (+/−) and (−/−) cortical neurons at DIV 14. Scale bars: 100 nm.
(F) Analysis of morphological features of synapses from all genotypes of neurons. The length of the active zone (AZ), the width of the synaptic cleft (space of cleft) and the averaged diameter of synaptic vesicles were measured, and no significant differences (NS) were found across all genotypes of neurons. Number of vesicles relative to its AZ length or terminal area was also compared among all genotypes of neurons. Significant decreases were only observed in (−/−) neurons for the density of docked vesicles (p=0.045, *u* test) and the density of total vesicles (p=0.016, *u* test).

NIH-PA Author Manuscript

NIH-PA Author Manuscript

NIH-PA Author Manuscript

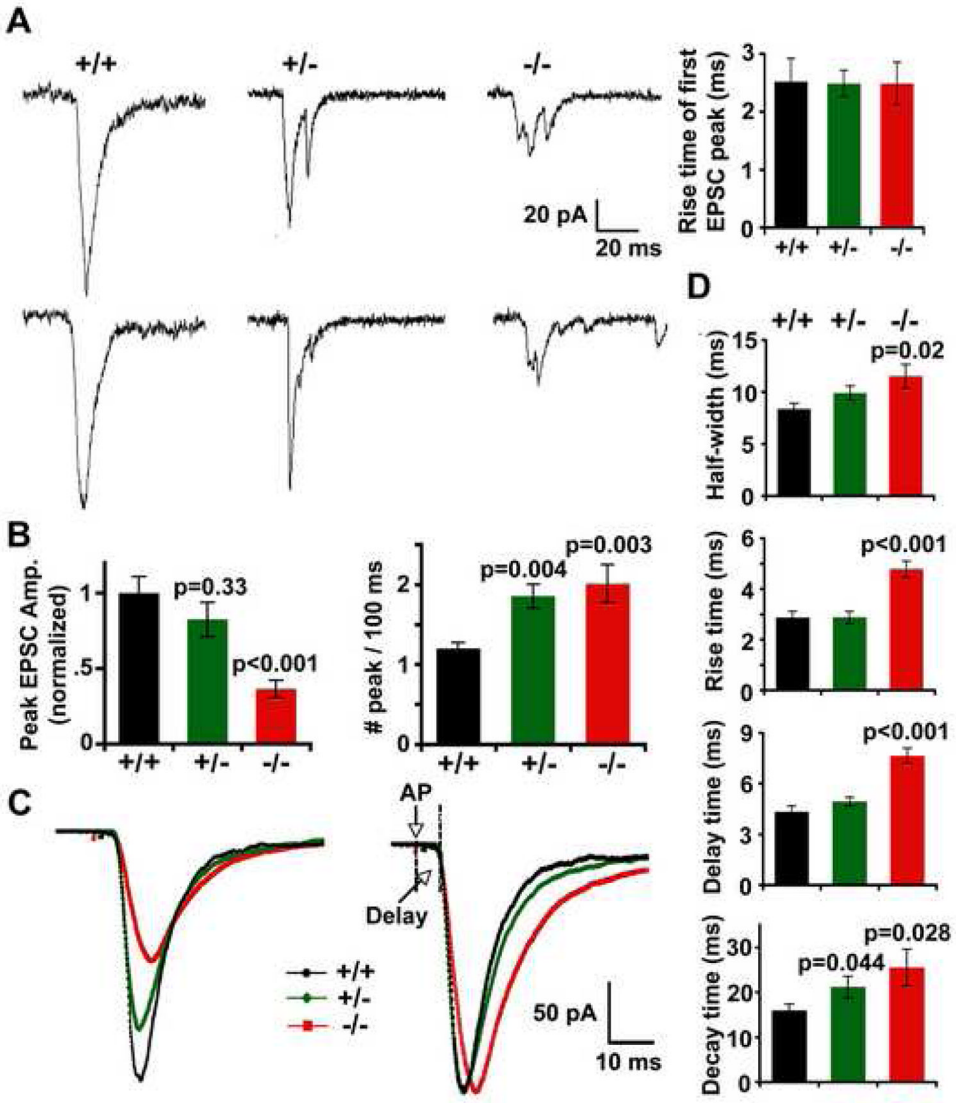

Figure 3. Deletion of *snapin* reduces the EPSC size and slows the EPSC kinetics

(A) Representative AMPA-EPSCs by paired whole-cell recordings from *snapin* (+/+), (+/−) and (−/−) cortical neurons in culture. Note that single-peaked EPSCs reflecting synchronized synaptic vesicle fusion became smaller and multi-peaked with *snapin*-deficiency. Taking the first peak of each single EPSC from (+/−) and (−/−) neurons for analysis, the 10–90% rise time remained similar to their (+/+) controls (upper right).

(B) Bar graphs of normalized peak EPSC amplitudes (left) and number of peaks per 100 ms (right) from neurons of all genotypes. Relative to the wild-type control, *snapin* (−/−) neurons exhibited a remarkable decrease in the EPSC peak amplitude (0.36 ± 0.06, n=17, p<0.001), in parallel with a moderate decrease observed in (+/−) neurons (0.82 ± 0.12, n=22, p=0.33). Number of peaks per 100 ms for each neuron was averaged from 10 EPSCs evoked at 0.05 Hz. *Snapin* deficiency resulted in increased peak numbers from both (−/−) (n=10, p=0.003) and (+/−) (n=16, p=0.004) neurons in comparison to (+/+) (n=12).

(C) Overlay of averaged AMPA-EPSCs from (+/+) (black, n=8), (+/−) (green, n=13) and (−/−) (red, n=12) neurons (left), and the corresponding scaled traces (right), in which the peak values of EPSCs from *snapin* (+/−) and (−/−) neurons were scaled to that of (+/+) neurons. All

NIH-PA Author Manuscript

NIH-PA Author Manuscript

NIH-PA Author Manuscript

traces were aligned at the time points of their 10% rise in amplitude. Time of "Delay" was shown starting from the stimulus artifact (AP) to the point of 10% rise of averaged EPSC traces. (D) Bar graphs of half-width (top graph), 10–90 % rise time (second graph), delay time (third graph) and 10–90 % decay time (bottom graph) measured from the scaled traces. *Snapin* (−/−) neurons exhibited significant increases in half-width ($p=0.020$), rise time ($p<0.001$), time of delay ($p<0.001$) and decay time ($p=0.028$) relative to wild-type controls. A moderate increase in decay time ($p=0.044$; grouped *t* test, mean ± s.e.m) was also noticed in (+/−) EPSCs.

NIH-PA Author Manuscript

NIH-PA Author Manuscript

NIH-PA Author Manuscript

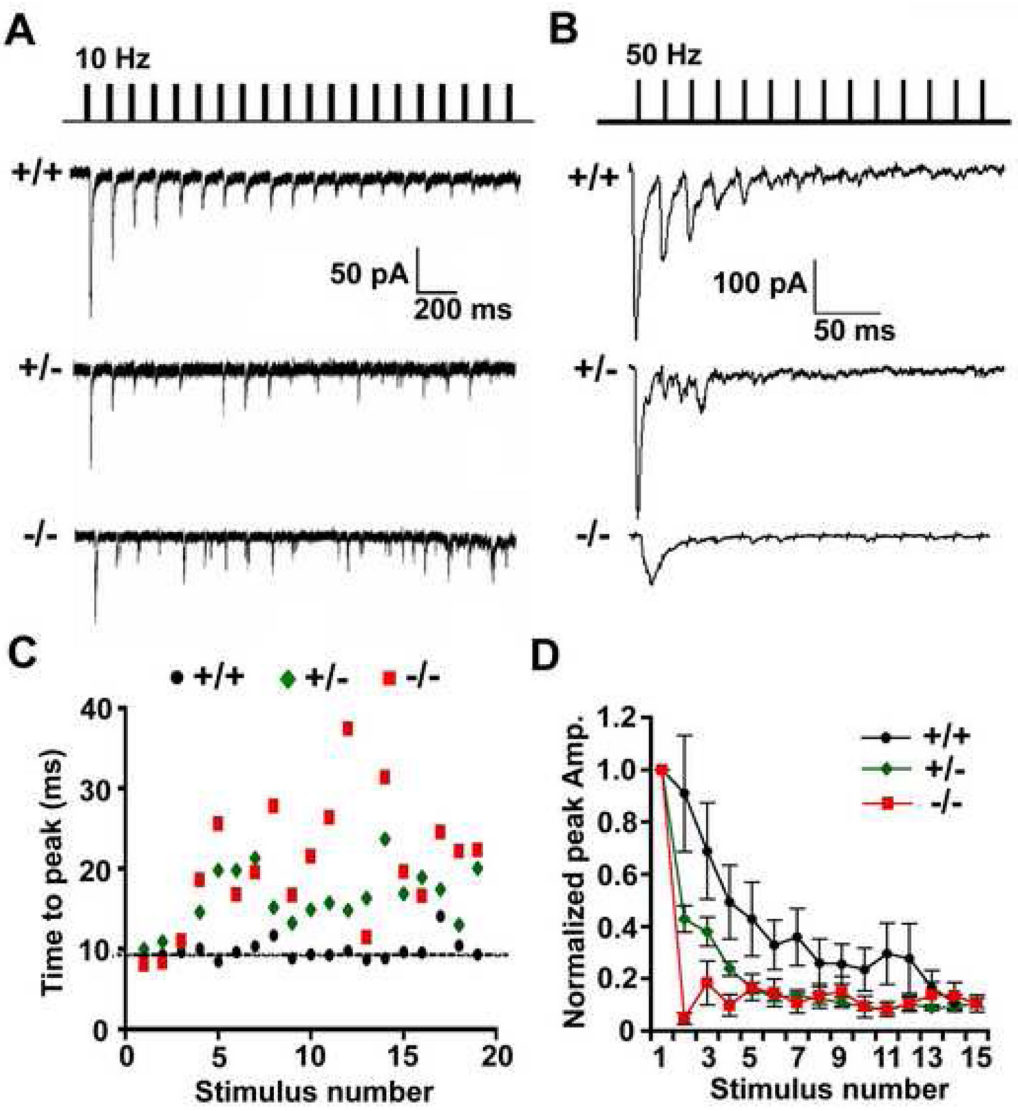

Figure 4. The precision and efficacy of synaptic transmission are impaired under high- frequency stimulations in both *snapin* (+/−) and (−/−) neurons

(A and B) Representative traces from *snapin* (+/+), (+/−) and (−/−) neurons at 10 Hz (A) and 50 Hz (B) stimulations.

(C) For each EPSC recorded at 10 Hz (as in A), the time-to-peak in 100 ms window (the time from each stimulus artifact to its peak) was plotted against stimulus number. Whereas the time-to-peak measured from (+/+) neurons remained at baseline throughout the stimulus train, those from (+/−) and (−/−) neurons exhibited more severe delays and larger variability.

(D) Normalized EPSC peak amplitudes plotted against stimulus number at 50 Hz stimulus train (as in B). Faster depression was seen in *snapin* (+/−) and (−/−) neurons. Data points as mean ± s.e.m.

NIH-PA Author Manuscript

NIH-PA Author Manuscript

NIH-PA Author Manuscript

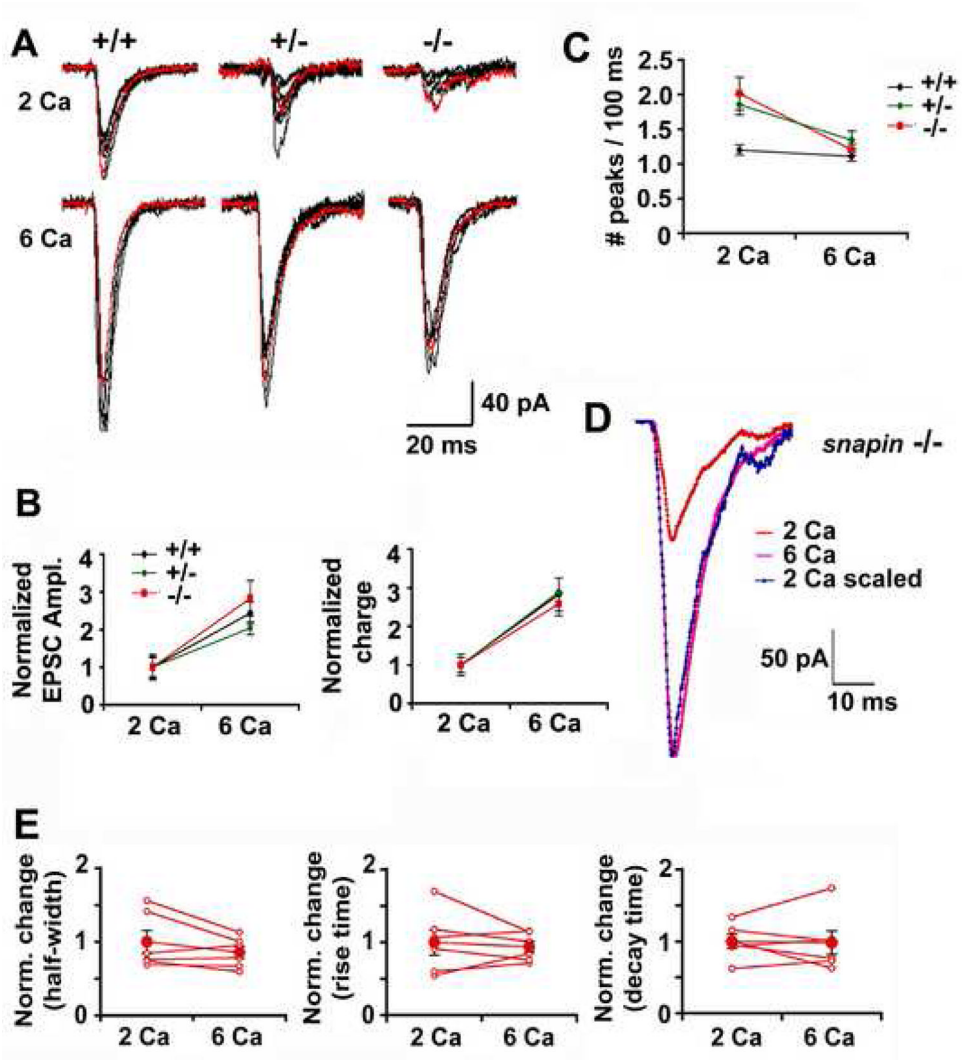

Figure 5. Elevated external calcium partially rescues the size but not EPSP kinetics

(A) Five superimposed single traces recorded from (+/+), (+/−) and (−/−) neurons when the recording chamber was perfused with 2 mM (upper) and 6 mM (lower) calcium solutions in sequence.

(B Relative increase in EPSC size (left panel) and total charge (right panel) when external calcium was elevated from 2 mM to 6 mM.

(C) Averaged number of EPSC peaks measured from (+/+) (n=17), (+/−) (n=20) and (−/−) (n=13) neurons in both 2 mM and 6 mM $[Ca^{2+}]_{ext}$ conditions. Note that increased peak number observed from *snapin* (+/−) and (−/−) neurons in 2 mM $[Ca^{2+}]_{ext}$ could be reduced to the (+/+) level when $[Ca^{2+}]_{ext}$ was elevated to 6 mM.

(D) Overlay of averaged AMPA-EPSCs recorded from a representative (−/−) neuron, when perfused with 2 mM and 6 mM $[Ca^{2+}]_{ext}$.

(E) Changes in AMPA-EPSC half-width (left), rise time (middle) and decay time (right) when increasing $[Ca^{2+}]_{ext}$ from 2 mM to 6 mM, plotted for 7 paired (−/−) neurons (open red circle) and their means (filled red circles). No significant differences in kinetics were observed (paired *t* test, mean ± s.e.m).

NIH-PA Author Manuscript

NIH-PA Author Manuscript

NIH-PA Author Manuscript

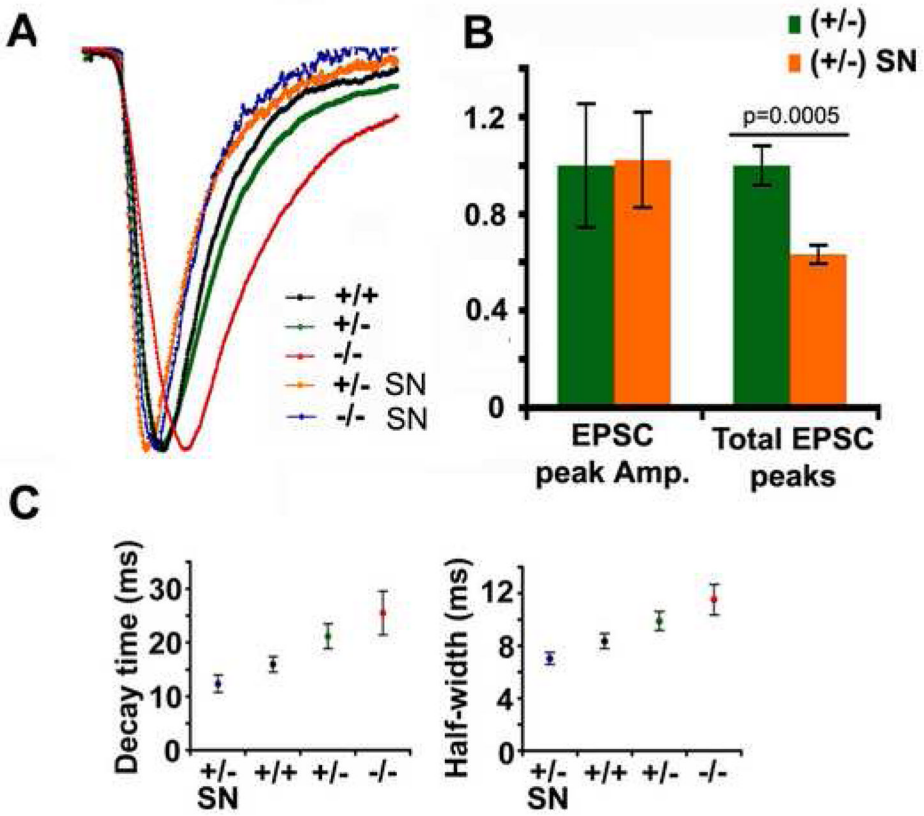

Figure 6. Snapin fine-tunes EPSC kinetics in a gene dose-dependent manner

(A) Overlay of scaled average AMPA-EPSCs from (+/+) (n=8), (+/−) (n=13), (−/−) (n=12) and rescued neurons by presynaptic expression of pIRES-EGFP-*snapin* transgene (+/− SN, n=8; −/−SN, n=10). Delayed EPSC kinetics found in *snapin* (+/−) and (−/−) neurons were not only effectively rescued, but also further accelerated relative to (+/+) neurons when Snapin expression was transiently elevated.

(B) The average amplitude and total number of peak EPSCs within 100-ms window. Note that average peaks in (+/−) neurons transfected with *snapin* transgene were remarkably decreased (0.63 ± 0.04, p=0.0005) as comparing to their non-tranfected controls.

(C) Gene-dose dependent change of EPSC decay time (left) and half-width (right) recorded from presynaptic *snapin* (−/−), (+/−), (+/+) neurons and (+/−) neurons rescued by transient expression of exogenous Snapin.

NIH-PA Author Manuscript

NIH-PA Author Manuscript

NIH-PA Author Manuscript

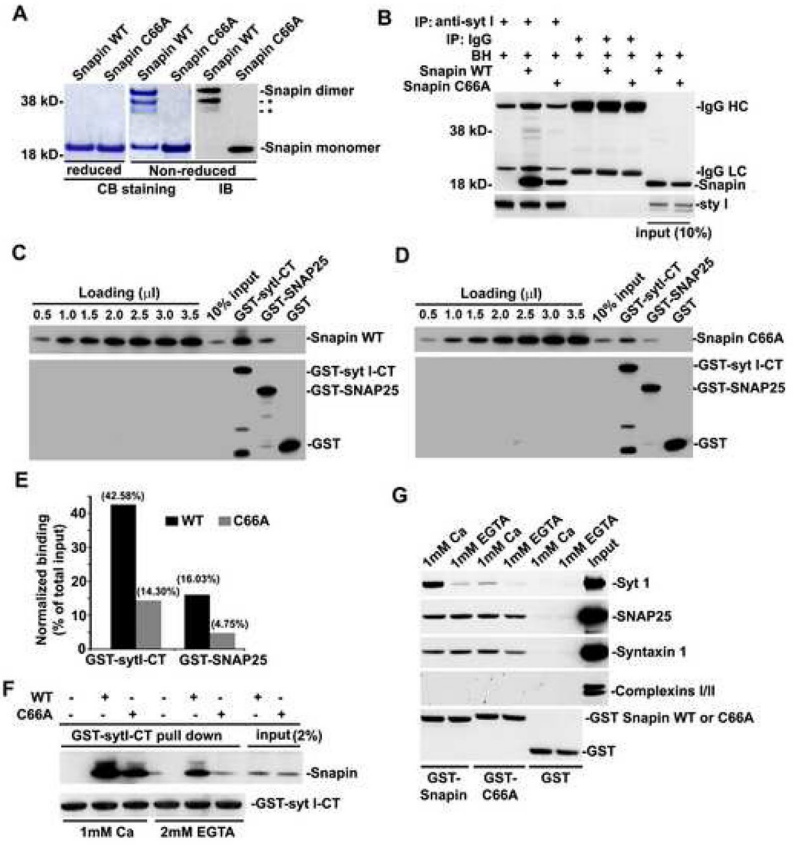

Figure 7. Snapin dimerization significantly enhances its interaction with SNAP-25 and Syt I

(A) Snapin forms a homodimer and Snapin-C66A is a dimerization-defective mutant. Purified His-tagged Snapin wild-type (WT) and its C66A mutant were separated on 4–12% SDS-PAGE under non-reduced or reduced conditions and stained with Coomassie Brilliant Blue (CB) or immunoblotted (IB) with an anti-Snapin antibody. Under non-reduced conditions, the majority of Snapin WT but not its C66A mutant migrated at the apparent molecular mass of 40 kD, while in reduced gels, they were both exclusively detected at ~20 kD. *: degraded Snapin dimer.

(B) Immunoprecipitation shows that Snapin C66A mutant reduces interaction with native Syt I from rat brain homogenates (BH). 1 μg of purified Snapin WT or C66A mutant were incubated with 50 μg of brain homogenates followed by immunoprecipitation (IP) with anti-Syt I or control IgG, and sequentially immunobloted with anti-Snapin and anti-Syt I.

(C-E) GST pull-down. GST-tagged cytoplasmic domain of Syt I (GST-syt I-CT), GST-SNAP-25, or GST control immobilized on glutathione-Sepharose beads were incubated with His-tagged Snapin WT (C) or C66A mutant (D). Bound proteins were immunobloted with antibodies against Snapin (upper) and GST (lower). Series dilutions of both Snapins were loaded on the same gels to serve as standard curves for semi-quantification of normalized binding relative to total input (E). Note that the Snapin dimerization-defective mutant significantly impairs its capability to stably interact with both Syt I and SNAP-25 *in vitro*.

(F) Elevated Ca^{2+} efficiently rescues the binding defect of Snapin C66A to Syt I *in vitro*. GST-sytI-CT immobilized on glutathione-Sepharose beads was incubated with His-tagged Snapin WT or C66A mutant under 2 mM EGTA or 1 mM Ca^{2+}. Bound proteins were detected using antibodies against Snapin (upper) and GST (lower).

(G) Ca^{2+} is required for GST-Snapin-C66A to pull down native Syt I from brain homogenates. GST-Snapin or its C66A mutant immobilized on glutathione-Sepharose beads was incubated

with 50 μg of rat brain homogenates in the presence of 1 mM Ca^{2+} or EGTA. Bound proteins were sequentially detected using antibodies against Syt I, SNAP-25, syntaxin 1, Complexin I/II, and GST from the same membrane after stripping between applications of each antibody as indicated. The experiments were repeated for three times.

NIH-PA Author Manuscript
NIH-PA Author Manuscript
NIH-PA Author Manuscript

NIH-PA Author Manuscript

NIH-PA Author Manuscript

NIH-PA Author Manuscript

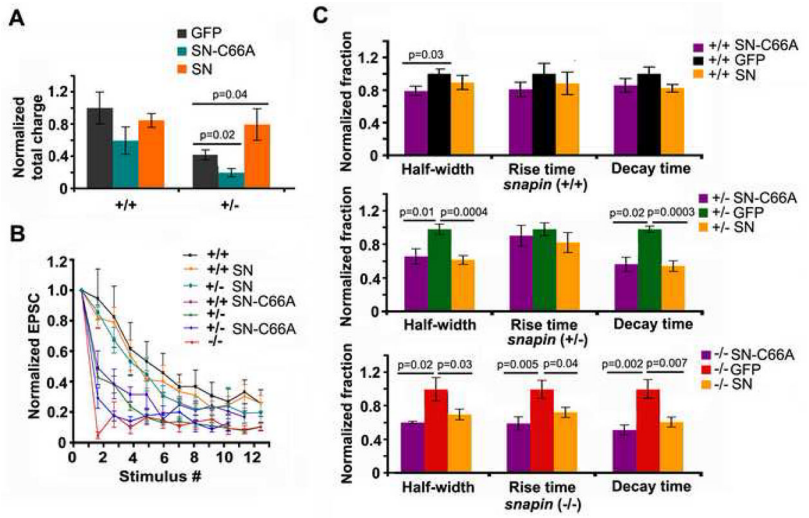

Figure 8. Dual roles of Snapin in synchronizing synaptic vesicle fusion and maintaining RRP size

(A) Relative changes in total charge transfer at 50 Hz, 0.8 s stimulation when pIRES-EGFP-Snapin-C66A (SN-C66A) or pIRES-EGFP-Snapin (SN) was expressed at the presynaptic neuron compared to their EGFP controls. Total charge transfer displayed changes in opposite directions when SN-C66A or SN was expressed in the presynaptic (+/−) neurons (GFP: 0.42 ± 0.06, n=11; SN-C66A: 0.20 ± 0.05, n=8, p=0.017; SN: 0.79 ± 0.19, n=9, p=0.037. *t* test).

(B) Normalized EPSC peak amplitudes plotted against stimulus number at 50 Hz stimulus train for *snapin* (+/+), (+/−) and (−/−) neurons, and for (+/+) and (+/−) neurons with presynaptic expression of either SN or SN-C66A. Note that SN-C66A expression resulted in faster decay in both (+/+) and (+/−) neurons, while Snapin expression reversed the decay kinetics in (+/−) neurons to reach the (+/+) level.

(C) Bar graphs of normalized EPSC half-width, 10–90% rise time and decay time plotted for *snapin* (+/+) (upper panel), (+/−) (middle panel) and (−/−) neurons (lower panel) when expressed with SN, SN-C66A or GFP control. In (+/+) neurons, no overall significant change was observed. In contrast, transient expression of SN in the presynaptic (+/−) and (−/−) neurons significantly decreased half-width (for +/−, 0.67 ± 0.05, p=0.0004; for −/−, 0.69 ± 0.06, p=0.032, *t* test) and decay time (for +/−, 0.55 ± 0.06, p=0.00006; for −/−, 0.60 ± 0.06, p=0.0066, *t* test) of AMPA-EPSC relative to their GFP controls. SN-C66A expression rescued EPSC kinetics in both half-width (for +/−, 0.70 ± 0.09, p=0.014; for −/−, 0.60 ± 0.02, p=0.015, *t* test) and decay time (for +/−, 0.67 ± 0.10, p=0.017; for −/−, 0.51 ± 0.06, p=0.0019, *t* test) as effectively as expression of wild-type SN. In *snapin* (−/−) neurons, rise time was also remarkably decreased when expressing SN (0.72 ± 0.06, p=0.037) or SN-C66A (0.59 ± 0.08, p=0.0054) at the presynaptic neurons relative to snapin (−/−) neurons expressing GFP control.